

H. D. Matthews · A. J. Weaver · K. J. Meissner
N. P. Gillett · M. Eby

Natural and anthropogenic climate change: incorporating historical land cover change, vegetation dynamics and the global carbon cycle

Received: 25 June 2003 / Accepted: 19 December 2003 / Published online: 18 March 2004
© Springer-Verlag 2004

Abstract This study explores natural and anthropogenic influences on the climate system, with an emphasis on the biogeophysical and biogeochemical effects of historical land cover change. The biogeophysical effect of land cover change is first subjected to a detailed sensitivity analysis in the context of the UVic Earth System Climate Model, a global climate model of intermediate complexity. Results show a global cooling in the range of -0.06 to -0.22 °C, though this effect is not found to be detectable in observed temperature trends. We then include the effects of natural forcings (volcanic aerosols, solar insolation variability and orbital changes) and other anthropogenic forcings (greenhouse gases and sulfate aerosols). Transient model runs from the year 1700 to 2000 are presented for each forcing individually as well as for combinations of forcings. We find that the UVic Model reproduces well the global temperature data when all forcings are included. These transient experiments are repeated using a dynamic vegetation model coupled interactively to the UVic Model. We find that dynamic vegetation acts as a positive feedback in the climate system for both the all-forcings and land cover change only model runs. Finally, the biogeochemical effect of land cover change is explored using a dynamically coupled inorganic ocean and terrestrial carbon cycle model. The carbon emissions from land cover change are found to enhance global temperatures by an amount that exceeds the biogeophysical cooling. The net effect of historical land cover change over this period is to increase global temperature by 0.15 °C.

1 Introduction

Changes in global climate in the latter half of the twentieth century represent a distinct anomaly in the historical climate record. The global temperature increase of 0.6 ± 0.2 °C since 1900 has occurred at a rate unprecedented in the last 1000 years (Houghton et al. 2001). The current global temperature is unmatched in the Holocene (the last 10,000 years), and indeed has not occurred since the peak of the last interglacial, some 126,000 years ago (Petit et al. 1999).

In the last several decades, the field of climate science has been motivated largely by the challenge to understand the changes that we are currently observing in the climate system. In the last decade, the global scientific community, as represented by the Intergovernmental Panel on Climate Change (IPCC), has sent a clear message that human activities are in large part responsible for the climate changes we are currently experiencing. Key among the identified causes of this global warming are elevated levels of greenhouse gases: levels that are unprecedented in the last 420,000 years (Houghton et al. 2001, Petit et al. 1999).

Numerous studies have identified processes that can act to force changes in global climate. Anthropogenic influences, of which greenhouse gases are known to be the most significant, also include emissions of sulfate aerosols and human land cover change, as well as numerous smaller forcings such as stratospheric ozone depletion, black and organic carbon aerosols and jet contrails. Natural climate forcing processes include solar variability due to sunspot and other solar cycles, long-term changes in solar orbital parameters, and intermittent volcanic eruptions (Hansen et al. 1998, Houghton et al. 2001). Many of these processes and their effects on global climate are very well understood, and are not discussed in detail here (see e.g. Ramaswamy et al. 2001). One of the less well understood anthropogenic influences on climate is that

H. D. Matthews (✉) · A. J. Weaver · K. J. Meissner
N. P. Gillett · M. Eby
School of Earth and Ocean Sciences, University of Victoria, PO
Box 3055, Victoria, BC, V8W 3P6, Canada
E-mail: damon@ocean.seos.uvic.ca

of historical land cover change, which is the focus of this study.

The radiative effect of historical land cover change on climate was highlighted in a review of contemporary climate forcings by Hansen et al. (1998). Here, the authors conclude that the radiative forcing due to historical land cover change is $-0.2 \pm 0.2 \text{ W/m}^2$, resulting in a global cooling of $-0.14 \text{ }^\circ\text{C}$. The primary mechanism for this cooling is the increase in surface albedo that results when forest land cover types are replaced by cropland or pasture. This effect is particularly important in higher latitudes, where the snow-masking effect of vegetation is greatly reduced as a result of forest to cropland conversion (Hansen et al. 1998).

Several studies using reduced complexity climate models have also found a global cooling as a result these biogeophysical effects of historical land cover change. Brovkin et al. (1999) and Bauer et al. (2003) determined historical deforestation over the last millennium to have induced a global cooling of $-0.35 \text{ }^\circ\text{C}$. Other studies have found smaller effects, such as $-0.1 \text{ }^\circ\text{C}$ over the last millennium (Bertrand et al. 2002) or $-0.1 \text{ }^\circ\text{C}$ over the last 300 years (Matthews et al. 2003). All of these studies prescribed transient scenarios of land cover change over the period of time studied.

A number of equilibrium studies using atmospheric general circulation models (AGCMs) have also noted both regional and global effects. Betts (2001) found that the global temperature is only $-0.02 \text{ }^\circ\text{C}$ cooler in a comparison between present-day and pre-industrial vegetation equilibria, but noted stronger cooling (in the range of -1 to $-2 \text{ }^\circ\text{C}$) in the northern mid-latitudes in winter and spring. Bounoua et al. (2002) and Zhao et al. (2001) also determined globally averaged changes to be very small, but found significant regional and seasonal changes, both warming and cooling. Chase et al. (2000, 2001) found land cover change to have significant impacts on atmospheric circulation, particularly in the Northern Hemisphere winter, and further argued that near-surface regional temperature anomalies due to land cover changes may be of similar magnitude to transient changes due to carbon dioxide and sulfate aerosol forcing. Govindasamy et al. (2001), in an AGCM/slab-ocean equilibrium comparison found a global cooling of $-0.25 \text{ }^\circ\text{C}$, and went so far as to suggest that reconstructed Northern Hemisphere cooling trends over the past millennium could be largely the result of anthropogenic land cover change.

Compounding the issue of the climatic effect of land cover change is the contribution of land conversion to climate warming as a result of large emissions of carbon dioxide (Bolin et al. 2000). A number of studies have provided estimates of emissions associated with land cover change; most recently Houghton (2003) estimates a total release of 156 GtC between 1850 and 2000. Only a couple of modelling studies have attempted to assess the net effect of land cover change on climate by including both the biogeophysical effects of changes to the land surface as well as the biogeochemical effects of

carbon emissions (Betts 2000; Claussen et al. 2001). Betts (2000) compared the biogeochemical and biogeophysical effects of reforestation in northern mid-latitudes, and found that in some cases, biogeophysical warming exceeded the counteracting effects of carbon uptake. Claussen et al. (2001) demonstrated that the net effect of land cover change, either in the case of deforestation or afforestation, is highly dependent on the latitude at which land cover change occurs: at high northern latitudes, there is a positive relationship between the amount of forest cover and temperature, whereas in the tropics and subtropics, the relationship is negative. These studies infer that deforestation occurring at high latitudes would likely result in a net cooling, whereas in the tropics, a net warming is more likely.

In a recent sensitivity study, Myhre and Myhre (2003) suggest that model results of the effect of land cover change are highly sensitive to specified vegetation datasets and surface albedo values. Considering the range of vegetation albedo values and land cover change datasets available, they found a large range of radiative forcings: between -0.6 and $+0.5 \text{ W/m}^2$, although they noted that positive radiative forcing results only occurred using extreme combinations of land cover change scenarios and surface albedo values, which are likely unrealistic. Nevertheless the large range of land cover change radiative forcing presented in their study, as well as the range of radiative forcing and temperature results from previous studies of land cover change highlight the need for further study in this area.

Matthews et al. (2003) describe a preliminary exploration of the radiative effect of land cover change using the UVic Earth System Climate Model. The current study builds on this work by presenting a range of land cover change experiments using varying datasets and model configurations. Section 2 describes the UVic Earth System Climate Model and the modifications made for the purposes of this study. The land cover change equilibrium experiments are described and presented in Sect. 3, highlighting the important processes and model sensitivities found in this study. In Sect. 4, the transient effect of land cover change forcing is placed in the context of other anthropogenic (greenhouse gases and sulfate aerosols) and natural (volcanoes, solar variability and orbital changes) forcings. This section also addresses the detectability of land cover change in the historical temperature record in relation to other model forcings. Section 5 presents the results of transient climate runs using a more comprehensive land surface and dynamic vegetation model. The net effect of historical land cover change is addressed in Sect. 6 by way of coupled terrestrial and inorganic ocean carbon cycle models.

2 Model description

The model used in this study is a version of the UVic Earth System Climate Model (ESCM). This is an intermediate complexity coupled atmosphere/ocean/sea-ice climate model, and is described in detail in Weaver et al. (2001). The ocean component of the model is

version 2.2 of the GFDL Modular Ocean Model (Pacanowski 1995), a general circulation ocean model with 19 vertical levels. The atmosphere is a vertically integrated energy/moisture balance model comprising a single atmospheric layer that captures well the climatic mean state in the absence of atmospheric variability. A prescribed lapse rate is applied over orography on land to determine the atmospheric temperature at which precipitation occurs, either in the form of rain or snow (Weaver et al. 2001). In a single-layer atmosphere however, this biases the model toward very high precipitation over mountains: the model's hydrological cycle over land is improved by reducing the lapse rate used to generate precipitation in the model (see Fig. 1). Surface wind stress as well as vertically integrated atmospheric winds used for advection of moisture are specified from NCEP reanalysis data. A dynamic wind feedback parametrisation allows for wind perturbations to be applied when simulating past climates. Sea-ice is represented by a dynamic/thermodynamic model, as described in Bitz et al. (2001). The coupled model has a resolution of 3.6° in longitude and 1.8° in latitude, and conserves both energy and water to machine precision without the use of flux adjustments (Weaver et al. 2001).

The version of the UVic ESCM used in this study carries a number of differences from that described in Weaver et al. (2001). First is an enhanced radiative transfer model to allow for the separation of the planetary albedo used in previous versions of the model into a surface and atmospheric component. Second, is the inclusion of two independent land surface models: the first modelled after the bucket model of Manabe (1969), and the second a modified version of the MOSES (Met Office Surface Exchange Scheme) model (Cox et al. 1999). Third, modifications are made to allow for the inclusion of volcanic and sulfate aerosols. Fourth, the dynamic vegetation model TRIFFID (top-down representation of interactive foliage and flora including dynamics, Cox 2001) is coupled to the UVic ESCM. Last, the terrestrial carbon cycle component of TRIFFID and the inorganic ocean carbon cycle described in Weaver et al. (2001) are coupled. These model improvements are described in the following sections.

2.1 Radiative transfer model

In previous versions of the UVic ESCM, a zonally averaged planetary albedo, $\alpha_{p(z)}$, was specified according to the parameters given in Graves et al. (1993). The net shortwave radiation at the surface was calculated as:

$$\downarrow SW = (1.0 - \alpha_{p(z)}) \cdot I_s \quad (1)$$

where I_s is the incident shortwave radiation at the top of the atmosphere. For the current study, it was necessary to incorporate a more detailed radiative transfer model that would include an explicit representation of surface albedo and a subsequent calculation of a two-dimensional planetary albedo field.

The approach chosen was based on the theory outlined in Haney (1971) and illustrated in Gill (1982, p 10), where planetary albedo (α_p) is calculated as a function of surface albedo (α_s), atmospheric albedo (α_a) and atmospheric absorption (A_a):

$$\alpha_p = (1 - \alpha_a)(1 - A_a)\alpha_s + \alpha_a \quad (2)$$

In this radiative transfer model, atmospheric albedo is made up of a clear sky albedo (set to 0.08) and a cloud albedo, which makes up the majority of the total albedo of the atmosphere. As the UVic ESCM does not model clouds explicitly, Eq. (2) was rearranged to solve for a zonally averaged atmospheric albedo given inputs of specified zonally averaged snow-free surface albedo, zonally averaged planetary albedo and atmospheric absorption:

$$\alpha_{a(z)} = \frac{\alpha_{p(z)} - \alpha_{sf(z)}(1 - A_a)}{1 - \alpha_{sf(z)}(1 - A_a)} \quad (3)$$

Zonally averaged planetary albedo ($\alpha_{p(z)}$) is taken as in previous versions of the UVic ESCM from Graves et al. (1993). Snow-free

surface albedo for this calculation ($\alpha_{sf(z)}$) is specified from ISLSCP data (Sellers et al. 1996) with ocean albedo increasing from 0.06 equatorward of 30° to 0.17 poleward of 70° . Atmospheric absorption (A_a) is set to a constant of 0.3.

Once a zonally averaged atmospheric albedo is obtained, it is inserted into Eq. (2) which becomes:

$$\alpha_p = (1 - \alpha_{a(z)})(1 - A_a)\alpha_s + \alpha_{a(z)} \quad (4)$$

Surface albedo is now generated by the land surface model and is allowed to change as a function of snow, ice or changing vegetation distributions. With atmospheric albedo held zonally constant, a new planetary albedo field can be calculated. The net shortwave radiation at the surface becomes:

$$\downarrow SW = (1.0 - \alpha_p) \cdot I_s \quad (5)$$

where α_p is now a two-dimensional field which reflects the underlying spatial variation in surface albedo. A zonally constant atmospheric albedo implies that clouds are not represented dynamically in the model. As such, feedbacks between changing climate and clouds are not included.

2.2 Land surface models

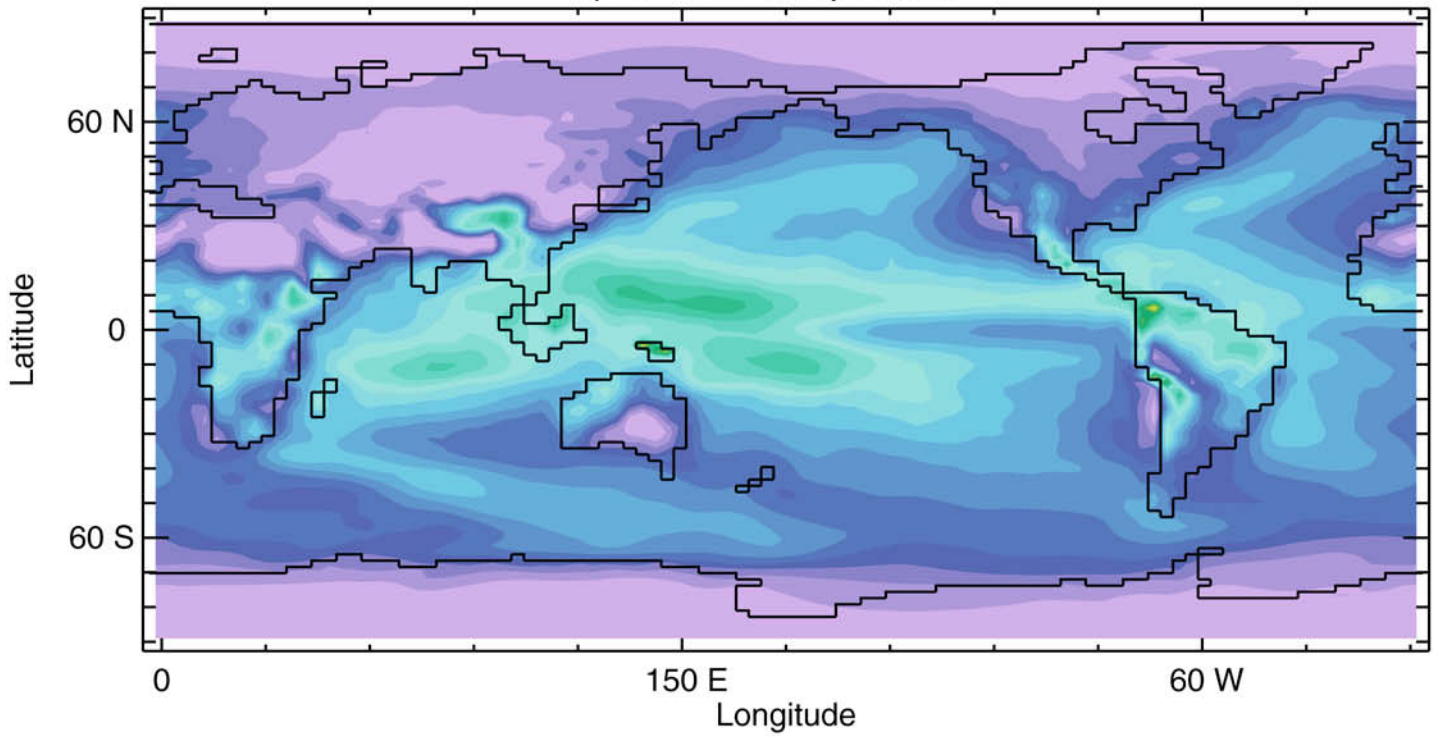
2.2.1 Modified bucket model

The land surface model described in this section and in Appendix 1 is used for all model runs presented in Sects. 3 and 4. Its basis is the simple bucket model of Manabe (1969), although it carries a number of modifications. The model uses a spatially uniform 15 cm bucket on land as a representation of the moisture holding capacity of the soil. Runoff occurs only when the bucket is full and the moisture holding capacity of the soil has been exceeded. Evapotranspiration is parametrised by a bulk formulation that includes a variable aerodynamic surface resistance, calculated from a specified roughness length (z_0), as well as the option of a specified surface resistance (r_s). This additional surface resistance represents the role that vegetation plays in moderating moisture fluxes to the atmosphere. The values of surface resistance chosen for this study follow the relative magnitudes of those given by Dickinson (2001), but have been reduced in absolute magnitude to put them in the range of those given by Cox et al. (1999). As there is significant discrepancy between these two sources, a compromise was chosen to allow some reasonable variability between vegetation types, while at the same time producing a climatology for evapotranspiration that is comparable to reanalysis data (see Fig. 2).

Vegetation is specified in the land surface model using the vegetation data set of DeFries and Townsend (1994). Eight vegetation types have been chosen to represent the range of vegetation provided in the dataset (shown in Table 1), noting that cropland differs from grassland/savanna only in its surface resistance. In the absence of cropland, a single vegetation type is specified at each gridcell, and in addition to surface resistance, the vegetation type determines the roughness length and the surface albedo. The values for these two parameters were determined by spatially and annually averaging roughness length and surface albedo data fields provided by Sellers et al. (1996) according to the specified vegetation types. These vegetation type-dependant parameter values are shown in Table 1, and are quite consistent with values given in the literature (see e.g. Wilson and Henderson-Sellers 1985; Cox et al. 1999; Dickinson 2001).

The snow/ice albedo in this model is set to 0.45. Variable snow masking depths (SMD, also shown in Table 3) allow for a linear transition from a snow-free surface albedo to the albedo for snow or sea-ice. Details of the parametrisations used in this version of the land surface model are described further in Appendix 1.

a) Model Precipitation



b) NCEP Precipitation

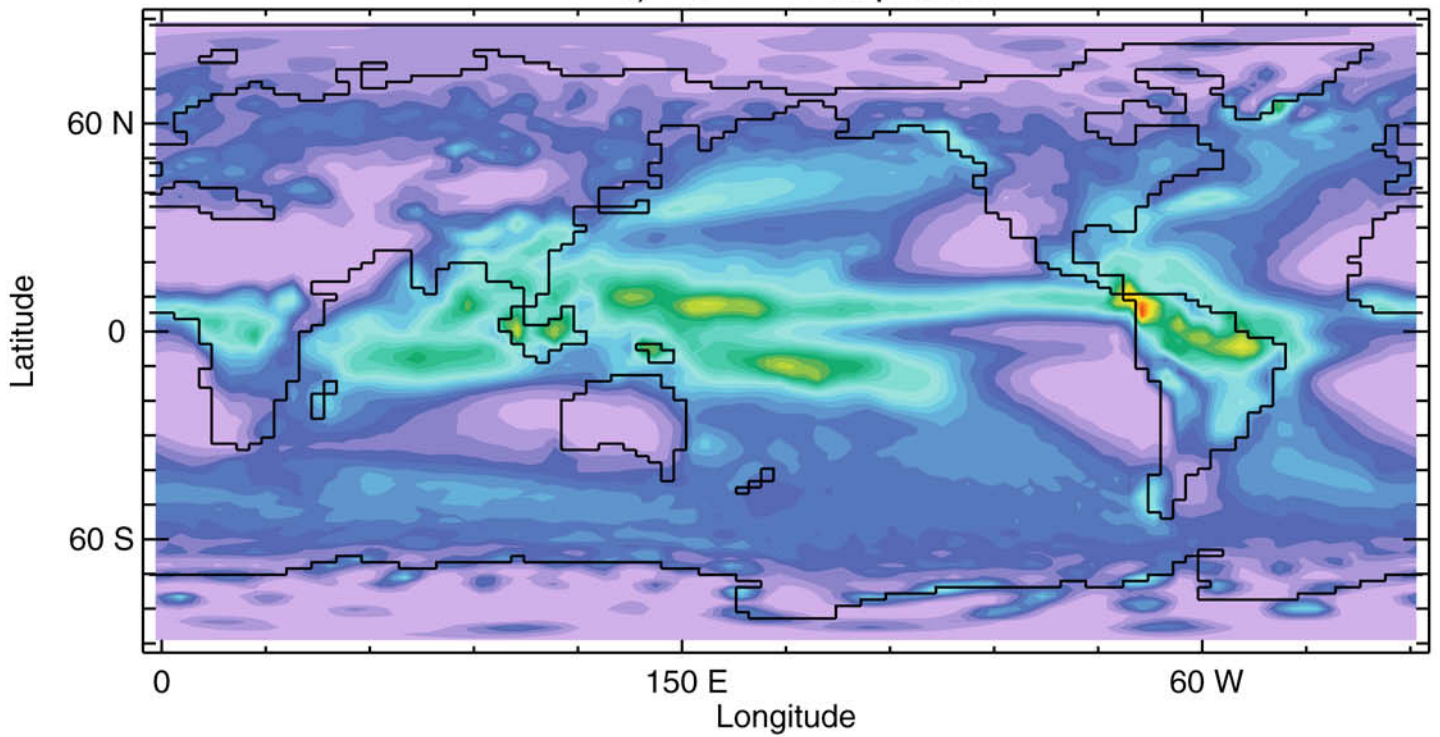




Fig. 1 a Modelled annual mean precipitation using the modified bucket land surface model (described in Sect. 2.2.1) compared to **b** NCEP annual mean precipitation

2.2.2 Modified MOSES land surface model

This version of the land surface model is used for all model runs presented in Sects. 5 and 6. This model includes a more complete representation of evapotranspiration, calculated as a function of the canopy resistance of five possible vegetation types per grid cell. Surface albedo is also calculated interactively as a function of vegetation distributions, leaf area index, leaf phenology and snow cover. Runoff is calculated by the method of Clapp and Hornberger (1978), using constant saturated hydraulic conductivity, soil moisture holding capacity and Clapp-Hornberger exponent. The model is a single soil layer version of MOSES, described in full in Cox et al. (1999). The version of the model, as coupled to the UVic ESCM is also described in detail in Meissner et al. (2003).

2.3 Natural and anthropogenic climate forcings

Sections 4 and 5 incorporate other natural and anthropogenic climate forcings into the UVic ESCM. Solar insolation is specified according to Lean et al. (1995) as a perturbation to the solar

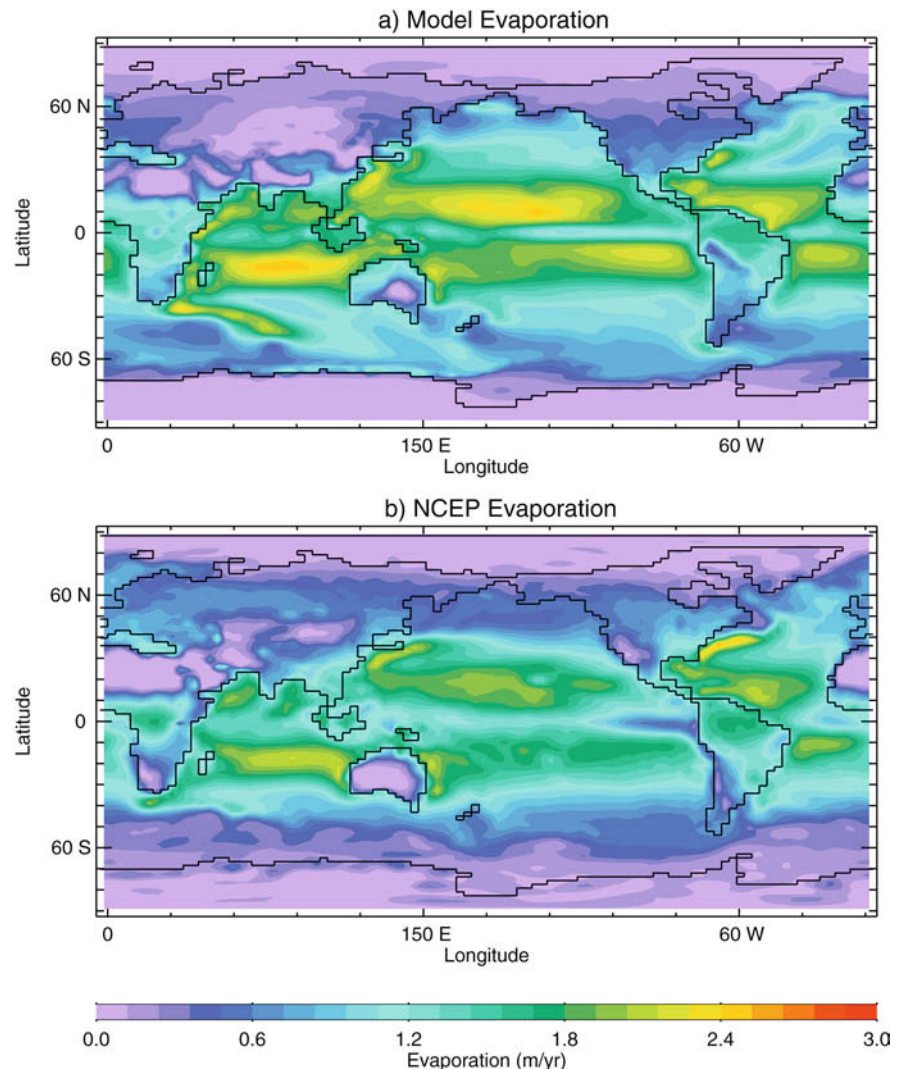
Table 1 Vegetation types and specified surface albedo (α_s) and roughness length (z_0) values as derived from DeFries and Townsend (1994) and Sellers et al. (1996). Surface resistances (r_s) and snow-masking depths (*SMD*) are taken from Dickinson (2001) and Cox et al. (1999)

Vegetation type	α_s	z_0 (m)	r_s (s/m)	<i>SMD</i> (m)
Tropical forest	0.13	2.86	75	10.0
Temperate/boreal forest	0.11	0.91	100	10.0
Grassland/savanna	0.17	0.11	100	0.1
Cropland	0.17	0.11	60	0.1
Shrubland	0.17	0.05	100	1.0
Tundra	0.20	0.04	100	0.1
Desert	0.28 ^a	0.04	100	0.01
Rock/ice	0.14	0.02	100	0.01

^aThis is the average of the albedo values for all desert points. Actual values are spatially variable and range from 0.2 to 0.38

constant. Solar orbital variation is calculated by the method of Berger (1978), as described in Weaver et al. (2001). Volcanic aerosols are specified as a globally averaged optical depth from the data of Robock and Free (1995) prior to 1850, and the data of Sato et al. (1993) from 1850 to 1999. These data are converted to a radiative forcing by the method used in Crowley (2000):

Fig. 2 a Modelled annual mean evaporation using the modified bucket land surface model with surface resistance included, compared to **b** NCEP annual mean evaporation



$$F = -k \cdot \tau \quad (6)$$

where the volcanic forcing (F) is a function of k (set to -30) and optical depth (τ). This forcing is applied as a negative perturbation to the downward shortwave incident at the top of the atmosphere.

Anthropogenic sulfate aerosol optical depth data are taken from Tegen et al. (2000) and Koch (2001). These data are applied as perturbation to the local surface albedo as:

$$\Delta\alpha_s = \beta\tau(1 - \alpha_s)^2 \cos(Z_{eff}) \quad (7)$$

where $\beta = 0.29$ is the upward scattering parameter, τ is the specified aerosol optical depth, α_s is the surface albedo and Z_{eff} is an effective solar zenith angle such that $\cos(Z_{eff})$ is the diurnally averaged cosine of the zenith angle (Charlson et al. 1991). Greenhouse gas forcing is applied as in Weaver et al. (2001), with greenhouse gas data (both CO_2 and non- CO_2 greenhouse gases) taken from Schlesinger and Malyshev (2001) and applied as a perturbation to outgoing longwave radiation. Land cover change forcing is described in Sect. 3.

2.4 Dynamic vegetation model

The dynamic terrestrial vegetation model used in Sects. 5 and 6 is the Hadley Center's TRIFFID model (Cox 2001). TRIFFID has been coupled interactively to the UVic ESCM and explicitly models five plant functional types: broadleaf trees, needleleaf trees, C_3 grasses, C_4 grasses and shrubs. The five vegetation types are represented as a fractional coverage of each gridcell, and compete amongst each other for dominance as a function of the model simulated climate. The coupling of TRIFFID to the UVic ESCM is described in detail in Meissner et al. (2003).

2.5 Global carbon cycle model

In addition to simulating vegetation distributions, TRIFFID calculates terrestrial carbon stores and fluxes. The net terrestrial flux of carbon to the atmosphere can be calculated as the difference between soil respiration and net primary production (NPP). As nitrogen limitation on plant growth is fixed, terrestrial carbon uptake is determined primarily as a function of changing atmospheric carbon dioxide and climatic conditions. This flux (in $\text{kg}/\text{m}^2/\text{s}$) is converted to or from ppmv using an atmospheric scale height of 8.5 km, which results in a conversion factor from GtC to ppmv of about 2.1. Carbon stores on land are represented by vegetation and soil carbon, and are updated by TRIFFID as a function of the flux of carbon to/from the atmosphere (a function of atmospheric CO_2 and climate) and changes in vegetation distributions (a function of climate).

The terrestrial carbon cycle is combined in this model with an inorganic ocean carbon cycle (Weaver et al. 2001) which simulates dissolved inorganic carbon as a passive tracer in the ocean, as well as carbon fluxes between the ocean and the atmosphere. At present the global carbon cycle represented in the UVic ESCM does not include a biological ocean component. However, in this we take the view as stated in Houghton et al. (2001): "Despite the importance of biological processes for the ocean's natural carbon cycle, current thinking maintains that the oceanic uptake of anthropogenic CO_2 is primarily a physically and chemically controlled process superimposed on a biologically driven carbon cycle that is close to steady state. This differs from the situation on land..." (p 199).

In Sect. 6 the UVic ESCM global carbon cycle model is enabled, and atmospheric carbon dioxide is computed prognostically as a function of ocean-atmosphere and land-atmosphere carbon fluxes. Anthropogenic emissions of carbon dioxide are specified from Marland et al. (2002); land-use emissions are specified from Houghton (2003). These emissions impose a perturbation to the equilibrium spin-up state, and the land and ocean carbon stores and fluxes respond dynamically to the imposed increase in

atmospheric carbon dioxide. The computed atmospheric carbon dioxide concentration is the resulting CO_2 in the atmosphere after global carbon sinks have responded to anthropogenic emissions.

3 Land cover change sensitivity experiments

In the UVic ESCM, historical land cover change is represented by the replacement of the natural vegetation type in a grid cell by a fractional area of cropland. When this occurs using the modified bucket land surface model, surface albedo, snow masking depth, roughness length and surface resistance are altered to reflect the modified land cover. In this section we present the results from a range of simulations investigating the radiative effect on global climate that results from specified historical land cover change. First we describe the two historical land cover datasets used in this study. We then describe the equilibrium model scenarios used to assess the sensitivity of global climate to historical land cover change in the context of the UVic ESCM. The experiments are listed in Table 2.

3.1 Dataset and experiment descriptions

3.1.1 Historical land cover change datasets

Two historical land cover datasets are used in this study. The first is that of Ramankutty and Foley (1999), which was also used by Matthews et al. (2003). This dataset consists of fractional cropland areas on a 1° grid for every year from 1700 to 1992, determined based on available historical records and interpolated linearly for intervening years. Accompanying the yearly croplands dataset is a potential or "natural" vegetation field, that forms the backdrop onto which croplands are applied (Ramankutty and Foley 1999, hereafter RF99). Implementation into a global climate model is relatively straightforward, as surface parameters are simply specified for the portion of each grid cell occupied by cropland.

The second dataset used is that of Klein Goldewijk (2001 hereafter the HYDE dataset). This dataset includes both historical croplands on a 0.5° grid as well as land used as pasture, and so arguably contains a somewhat more complete picture of historical land cover

Table 2 Equilibrium land cover change experiments

Experiment	Dataset	Variable surface parameters
RF:SM	RF99	SMD, albedo, roughness length
HYDE:SM	HYDE	SMD, albedo, roughness length
RF:SM + SR	RF99	SMD, albedo, roughness, surface resistance
RF:Alb	RF99	SMD, albedo (crops set to 0.17)
RF:Alb-	RF99	SMD, albedo (crops set to 0.15)
RF:Alb +	RF99	SMD, albedo (crops set to 0.20)
RF:GRL	RF99	albedo, roughness length

change. Furthermore, the placement of crop and pasture areas is determined from historical population densities, and so provides an independent corollary to RF99. Data is only provided, however, at 20 to 50 year intervals from 1700 to 1990, and consists of a single vegetation type at each grid cell.

3.1.2 Equilibrium climate runs

The experiments described in Matthews et al. (2003) provide a baseline to this work. In this study, we used the RF99 dataset with a version of the UVic ESCM as described there. The current study introduces two important modifications to the land surface model used in these previous experiments. The first is a snow masking scheme that allows for the albedo of snow covered land to vary according to the vegetation type. The second is a parametrisation of surface resistance, which allows for a more accurate representation of the evapotranspiration pathway and the effects on surface fluxes of moisture resulting from changing vegetation types. These modifications are described in Sect. 2.2.1 and Appendix 1.

Equilibrium runs are presented here using four different model/dataset configurations. First, the RF99 dataset is used including the variable snow masking scheme, but omitting the use of surface resistance for all vegetation types (RF:SM). The second experiment uses the same model configuration, but replaces the RF99 dataset with the HYDE dataset (HYDE:SM). Third, the RF99 dataset is used with both the snow masking scheme and the surface resistance parametrisation (RF:SM+SR). Fourth, the first experiment is repeated with only surface albedo and snow masking depth changing as a result of land cover change; other surface parameters (roughness length and surface resistance) are held constant (RF:Alb). Last, as the model was found to be highly sensitive to the specified cropland albedo (Matthews et al. 2003), the RF:Alb experiment was repeated twice replacing the cropland albedo (set to 0.17 in all other experiments) with values of 0.15 and 0.2 (denoted RF:Alb– and RF:Alb+ respectively). These albedo values are chosen to represent the extremes of cropland albedos represented in the literature (Myhre and Myhre 2003). Each experiment includes both a year 1700 simulation and a “present day” simulation, corresponding to the first and last land cover years available in each dataset. All equilibria arise from a 2000 year integration and are listed and described in Table 3. The final experiment listed in Table 3 (RF:GRL) corresponds to the experiment as reported in Matthews et al. (2003).

3.2 Results

Results of all equilibrium runs are presented in Table 3. The values shown here correspond to differences in globally averaged model variables between present day and year 1700 equilibria.

Table 3 Equilibrium changes in globally averaged temperature, precipitation, surface albedo and downward shortwave radiation between the present day and year 1700 equilibria

Experiment	T (°C)	P (mm/year)	Albedo	$\downarrow SW$ (W/m ²)
RF:SM	−0.13	−3.1	+0.0016	−0.199
HYDE:SM	−0.19	−7.6	+0.0023	−0.275
RF:SM+SR	−0.14	−0.8	+0.0016	−0.198
RF:Alb	−0.13	−2.6	+0.0016	−0.198
RF:Alb–	−0.06	−1.8	+0.0008	−0.075
RF:Alb+	−0.22	−3.3	+0.0023	−0.325
RF:GRL	−0.10	−3.3	+0.0010	−0.158

All experiments resulted in a global cooling and a decrease in precipitation. These changes were forced primarily by increases in surface albedo which resulted in a negative radiative forcing, as shown by decreases in net downward shortwave radiation at the surface. Globally averaged temperature changes range from −0.06 °C to −0.22 °C, depending on the model configurations and parameters used. Including pasture as well as croplands increases global cooling by −0.06 °C (HYDE:SM) compared to croplands alone (RF:SM). Including a parametrisation of surface resistance (RF:SM+SR) has very little effect on global temperature, but precipitation changes are much smaller compared to the case when surface resistance changes are ignored (RF:SM). This can be explained by the assigned r_s value for croplands, which is smaller than all other r_s values. In this scenario, crops are assumed to transpire more than other vegetation types, resulting in more precipitation over areas of land cover change that counteracts the reduced precipitation affected by global cooling.

Temperature changes on the model grid are shown in Fig. 3. Regional cooling resulting from land cover change ranges from 0 to −0.5 °C, reaching a maximum where large land cover changes (shown in Fig. 4) overlap with areas of seasonal snow cover. This is most clearly seen in Northern Europe and Asia. Also evident in Fig. 3 are regions where snow and sea-ice albedo feedbacks amplify local cooling, as seen off the coast of Antarctica and to some extent over northwest North America and in the North Atlantic. Overall, the majority of the cooling occurs over continental regions in the Northern Hemisphere. It should be noted here that as our atmospheric model does not simulate internal dynamics or variability, the results shown here are not masked by atmospheric noise. As such, even small changes are coherent and significant in the context of this model.

As in Matthews et al. (2003), the model is found to be very sensitive to specified surface albedo values. If cropland albedos are increased to 0.20 from the default value of 0.17, the global cooling is increased from −0.13 °C (RF:ALB) to −0.22 °C (RF:ALB+). If cropland albedos are decreased to 0.15, the global cooling is decreased to −0.06 °C (RF:ALB–). It is likely that differences in how surface albedo is affected by land cover

Fig. 3 Annual mean surface air temperature change on the model grid from year 1700 to present day for the equilibrium experiment RF:SM

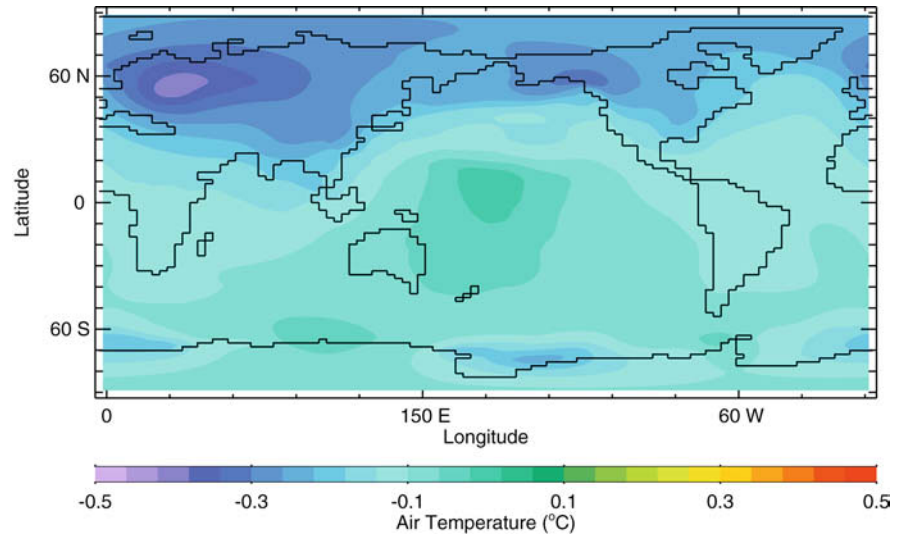
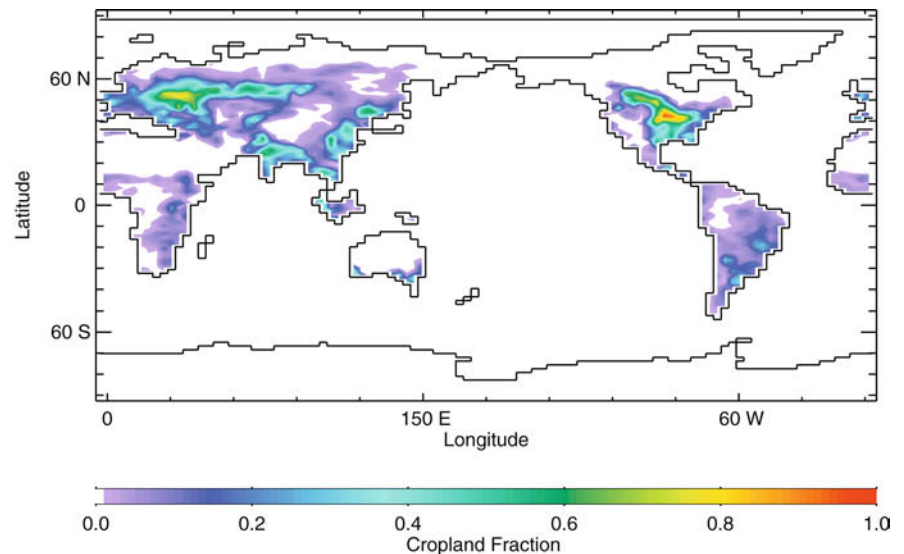


Fig. 4 Fractional cropland area change on the model grid from year 1700 to present day for the RF99 dataset



change in different models explains in large part the differences that are seen in model simulations of land cover change, a contention that is supported by the analysis of Myhre and Myhre (2003). There is also significant variability, however, in estimates of historical land cover change, and the interpretation of these data can account for discrepancy in model results. Bauer et al. (2003), for example, simulate a cooling over the past three centuries on the order of -0.3 °C, substantially higher than that found by our model, even accounting for reasonable surface albedo variation. Though Bauer et al. (2003) also use the RF99 dataset, they interpret cropland areas as deforested areas. In the simulations presented here, deforested areas are substantially less as in many instances, cropland is applied onto gridcells that in the “natural” vegetation field are already designated as grassland or savanna, resulting in no change in local surface albedo. It is likely this this difference in the model application of the RF99 crop-

lands data explains the difference between the results reported here and those of Bauer et al. (2003).

It is worth noting that excluding roughness length as a variable model parameter has very little effect on global temperature, although there are small differences in global precipitation (RF:Alb compared to RF:SM). The radiative forcing resulting from land cover change for all runs ranges from -0.075 (RF:Alb-) to -0.325 W/m² (RF:ALB+). This is well within the range of radiative forcing estimates provided in the literature (Hansen et al. 1998; Betts 2001; Myhre and Myhre 2003).

4 Natural and anthropogenic climate change

In this section, the transient effect of land cover change is compared to other natural and anthropogenic forcings. As reported in Matthews et al. (2003), the transient effect of land cover change from 1700 to present is very

similar to the equilibrium effect, a sign that there is very little oceanic cooling commitment associated with land cover change. For all transient runs reported in the following section, the model configuration used in experiment RF:SM+SR is chosen: the RF99 dataset is used (only croplands are accounted for) and all variable model parameter options are included.

The natural forcings considered are volcanic aerosols (VOLC), solar insolation variability (INS) and solar orbital changes (ORB). In addition to land cover change (LCC), the anthropogenic forcings of greenhouse gases (CO₂ and other non-CO₂ greenhouse gases) (GG) and sulfate aerosols (SUL) are included. The datasets and methods used for each of these forcings are outlined in Sect. 2.3. The transient effect of each forcing is considered individually (GG, SUL, LCC, VOLC, INS, ORB), and then in combinations of anthropogenic forcings only (ANTH), natural forcings only (NAT) and all model forcings (ALL). A control equilibrium was spun up for 2000 years using year 1700 conditions (solar constant, orbital parameters, land cover), with greenhouse gases set to 280 ppmv and volcanic and sulfate aerosols set to zero. Transient scenarios for each individual forcing and combination were run from the year 1700 to the year 2000.

4.1 Transient climate model runs

Figure 5 shows the results of transient runs driven by each individual model forcing. Greenhouse gas forcing results in a warming of 1.3 °C by the year 2000 compared to the control. Sulfate aerosols are assumed to be zero until 1850, after which they result in a cooling of -0.5 °C. Land cover change affects a cooling of -0.13 °C, very close to the equilibrium cooling of -0.14 °C found in the RF:SM+SR equilibrium experiment and consis-

tent with the notion that there is very little oceanic cooling commitment associated with land cover change.

Natural forcings can also be seen to have significant effects. The effect of volcanic aerosols is notable but periodic, with large cooling episodes associated with major volcanic eruptions. Mt. Pinatubo (1992), El Chichon (1982), Agung (1963) and Krakatau (1883) can all be seen clearly. The largest volcanic cooling is associated with Tambora (1815), said to have elicited the “year without a summer”, and a global cooling in the range of 1 °C (Robock 1994, 2000). A slight long-term cooling trend can be seen in the VOLC model run, though it is possible that this is simply a result of starting from a model spin-up that does not include volcanic aerosols. Solar insolation changes result in a significant warming over the 300 year model run, partly due to the fact that the year 1700 chosen for the equilibrium spin-up corresponds to a local insolation minimum in the Lean et al. (1995) dataset. The warming in the early part of the model run is probably artificially amplified as a result of this, although there is still an additional warming in the range of 0.2 °C over the period from 1800 to 2000. Solar orbital changes have virtually no effect on globally averaged temperature, and thus serve as a control transient run from 1700 to 2000.

It should also be noted that the linear sum of the individually forced climate responses (shown in Fig. 5 as the thin grey line) is almost indistinguishable from the model response to all model forcings together (ALL, thick black line). This demonstrates the linear additivity of climate model responses to individual forcings in the context of our model, a conclusion that has also been drawn from other modelling studies (see e.g. Ramaswamy and Chen 1997).

Combinations of forcings (ALL, NAT and ANTH) are shown for the period from 1850 to 2000 in Fig. 6 and compared to historical temperature data from Folland

Fig. 5 Transient model runs from 1700 to 2000 under the six individual model forcings, and for all-forcings combined. Greenhouse gas (GG) forcing only is shown in red, sulfate aerosols (SUL) in purple, land cover change (LCC) in orange, volcanic aerosols (VOLC) in blue, solar insolation (INS) in green and solar orbital (ORB) in cyan. A transient run forced by all model forcings together (ALL) is shown by the thick black line. The thin grey line shows the linear sum of the six individual model forcings, for comparison with the all-forcings model run

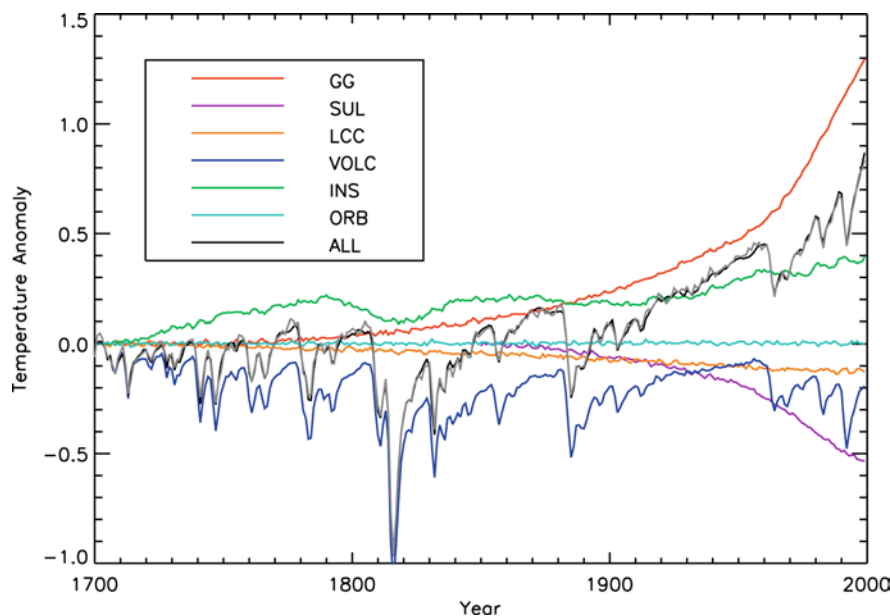
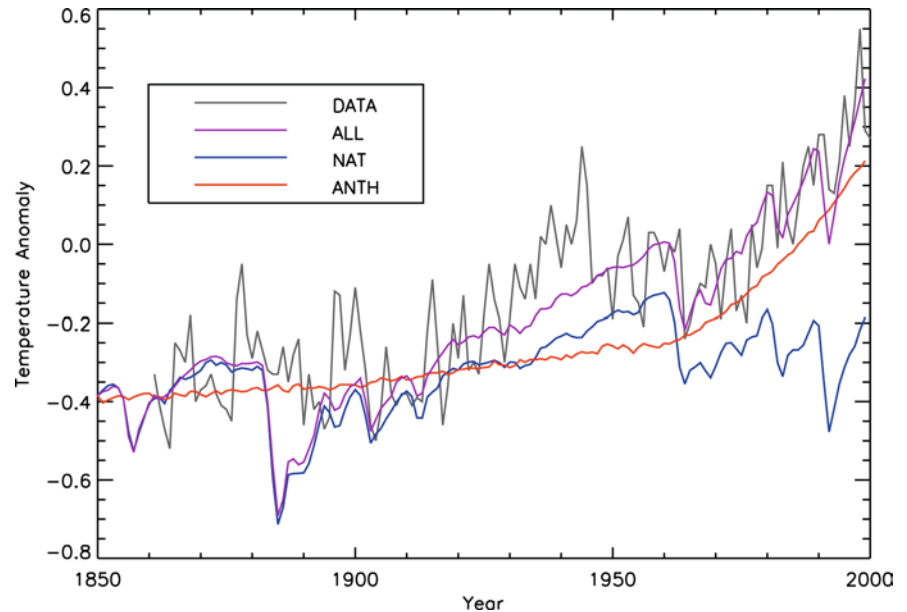


Fig. 6 All model forcings (*ALL*), natural (*NAT*) and anthropogenic (*ANTH*) combinations shown with global temperature data (*DATA*) for 1850 to 2000. *DATA* is shown in grey, *ALL* in purple, *NAT* in blue and *ANTH* in red. *ALL* and *DATA* are plotted as an anomaly against their respective 1961 to 1990 averages. *NAT* and *ANTH* are plotted such that they begin from the same point as *ALL*



et al. (2001). As can be seen by comparing the all model forcings run (purple line) with the temperature data (grey line), the UVic ESCM does an excellent job of reproducing the historical temperature trend in the absence of atmospheric variability. The twentieth century saw a warming of $0.8 \text{ }^\circ\text{C}$ in the all-forcings model run, consistent with the $0.6 \pm 0.2 \text{ }^\circ\text{C}$ warming cited by Houghton et al. (2001), and clearly in alignment with the temperature data shown in Fig. 6. The model produces a cooling in the 1960s associated with the Agung volcanic eruption, a cooling that is also seen in the data. The cooling in the 1940s is not reproduced by the model, suggesting that this temperature trend is likely the result of internal climate variability (such as El Niño/La Niña) that is not captured in our model. The data also does not show the large volcanic cooling in the 1880s associated with the Krakatau eruption, but this model/data discrepancy is consistent with other model simulations of this period (see for example, Stott et al. 2001). It is also quite possible that the reconstructed temperature records do not capture the transient effects of volcanoes well or that the optical depth changes inferred in the earlier portions of the volcanic records are not as good as more recent estimates.

Separation of model forcings into categories of natural forcings only (volcanic aerosols, solar insolation and orbital changes) and anthropogenic forcings only (greenhouse gases, sulfate aerosols and land cover change) reveal clearly the source of temperature changes seen in the all-forcings model run. The natural forcings only run (blue line in Fig. 6) shows a clear warming in the first half of the twentieth century as a result of a quiescence of volcanic activity and some increase in solar insolation, followed by a cooling trend in the latter half of the twentieth century, initiated and maintained by a series of large volcanic events. The anthropogenic forcings only run (red line in Fig. 6) shows a gradual

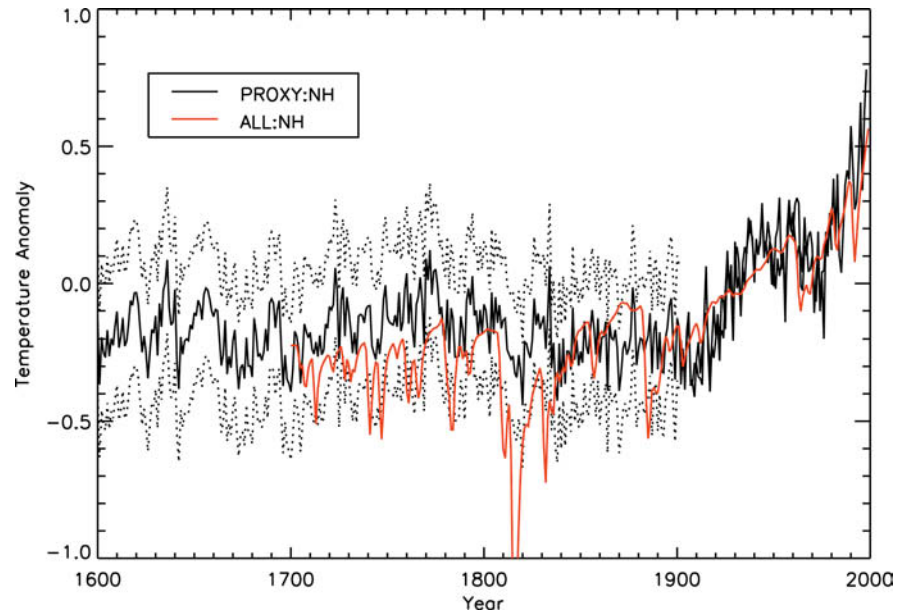
warming throughout the model run, but with a distinct acceleration of warming after 1960. These two model patterns combine in a linear fashion to generate the temperature trend seen in the all-forcings model run. Based on these results, we argue that the warming seen in the data in the early part of the century is a combination of greenhouse forcing and natural forcing, the cooling seen in the 1960s is a result of a resumption of volcanic activity, and the distinct warming in the latter half of the twentieth century can only be accounted for by greenhouse gas forcing. These conclusions are consistent with those found by Stott et al. (2001).

Figure 7 shows Northern Hemisphere temperatures from the all-forcings model run compared to the temperature reconstruction from Mann et al. (1999). While the strong volcanic signals seen in the model are not very well captured in the proxy data, the model results do fit within the error envelope of the proxy data prior to 1900, and track well the Northern Hemisphere temperature profile closely over the twentieth century.

4.2 Detection of climate change

Detection and attribution experiments represent an attempt to statistically detect trends seen in model output by comparing them to observations, and further to attribute the trends to external climate forcings. Recent detection and attribution studies have successfully attributed twentieth century temperature changes to greenhouse gas and sulfate aerosol forcing (Stott et al. 2001) as well as to changes in volcanic aerosols and solar irradiance (Jones et al. 2003). Hegerl et al. (2003) have also applied detection and attribution methods to longer proxy records in an effort to detect volcanic, solar and greenhouse gas signals in hemispherically averaged temperature proxies. In this section we apply the optimal

Fig. 7 All model forcings (*ALL*) compared to Northern Hemisphere temperature reconstruction (*PROXY*). Dotted lines indicate two standard deviations for the proxy data prior to 1900. Both proxy data and model results are plotted as anomalies against their respective 1902 to 1980 averages



fingerprint detection method (Tett et al. 1999) to UVic ESCM output of twentieth century temperature change to assess the detectability of changes forced by land cover change in comparison to all other model forcings.

Figure 8 shows the results of the detection and attribution experiment on model output from transient runs of land cover change and all other model forcings regressed against observations of the period from 1896 to 1996 (Jones 1993). Results are derived using an ordinary least squares regression of decadal mean T4 spherical harmonic temperatures (1896–1996) with a 10 EOF (empirical orthogonal function) truncation (Tett et al. 1999). Natural variability was estimated from the CGCM2 control simulation (Flato and Boer 2001). As can be seen on the horizontal axis of Fig. 8, the combination of all model forcings is very well detected, with a regression coefficient very close to 1. The effect of land cover change also carries a regression coefficient very close to 1, but the error bars are too large to make this forcing statistically detectable. We conclude that cooling due to land cover change in the twentieth century (about -0.05 °C) is too small to be detected statistically in observed trends. This experiment was repeated using the Mann et al. (1999) Northern Hemisphere temperature data for the period from 1700 to present. Although the error bars on the effect of land cover change were notably smaller, the signal was still not statistically detectable.

5 Dynamic vegetation

In this section we present transient runs using the UVic ESCM coupled to the modified MOSES land surface model (Sect. 2.2.2) and the dynamic terrestrial vegetation model TRIFFID (Sect. 2.4). Recent development of global dynamic vegetation models has allowed for the

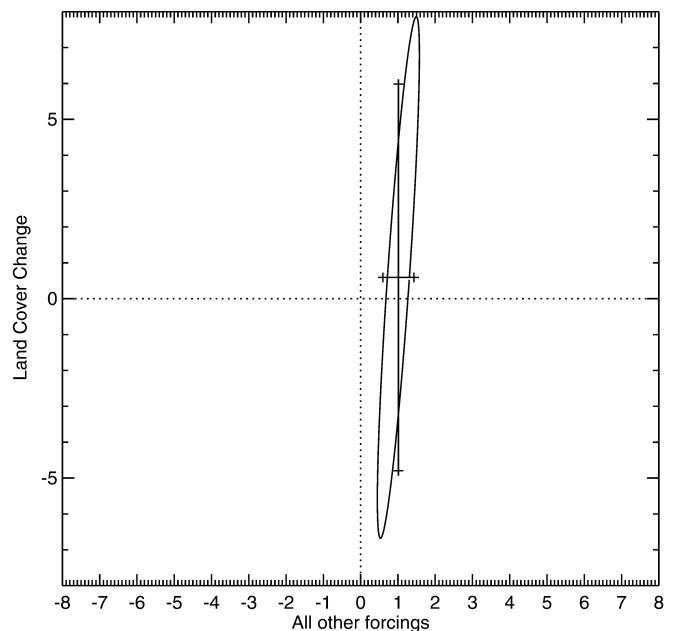


Fig. 8 Regression coefficients for land cover change and all other model forcings regressed against observations

study of how changing vegetation distributions as a function of climate could feed back to climate change (Cramer et al. 2001). In this section, we explore the role of vegetation dynamics as a feedback within the climate system in the context of twentieth century climate change, as well as in transient simulations of land cover change over that past 300 years. As in the previous versions of the model, land cover change is prescribed from the RF99 dataset as a fractional area of cropland in each gridcell. Now that vegetation is dynamic rather than prescribed, the prescribed land cover change allocates a portion of each grid cell where only grass plant

Fig. 9 All model forcings transient run from 1880 to 2000 compared to data for: previous model version (*ALL*), model version including MOSES and TRIFFID but holding vegetation constant (*ALL:CONST*) and model including MOSES and TRIFFID and dynamic vegetation (*ALL:DYN*)

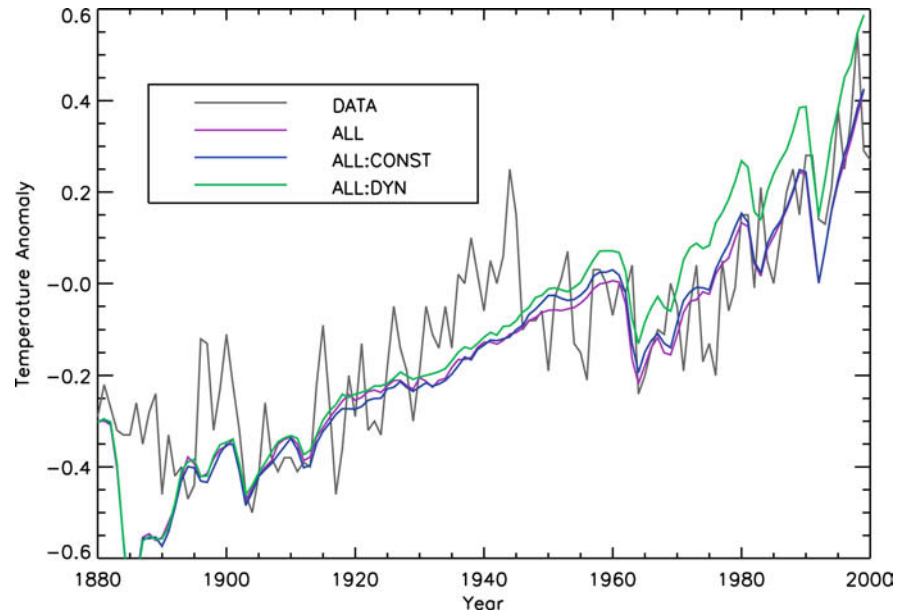
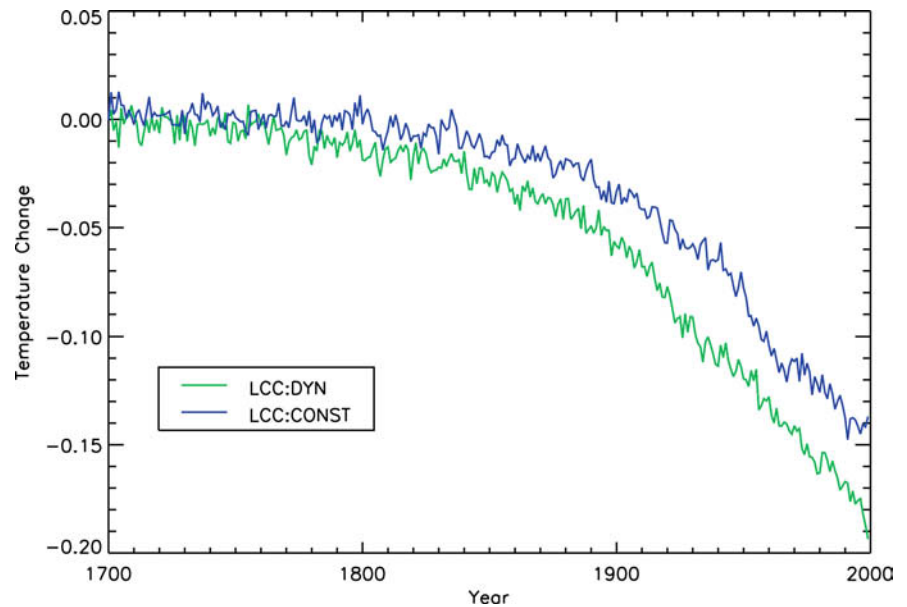


Fig. 10 Transient runs from 1700 to 2000 forced by land cover change alone for the model including MOSES and TRIFFID, with constant vegetation (*LCC:CONST*) compared to dynamic vegetation (*LCC:DYN*)



functional types (C_3 or C_4 grasses) are allowed to grow. The remaining plant functional types (trees and shrubs) compete for space along with grass types in the unallocated portion of the grid cell.

Figure 9 shows the all model forcing results for the twentieth century portion of the 300-year transient runs. Two new model runs are presented here: the first allows vegetation to respond dynamically to climate (*ALL:DYN*), and the second holds vegetation fixed at simulated pre-industrial distributions (*ALL:CONST*). These two runs are plotted in comparison to the previous all-forcings run (Sect. 4) without the dynamic vegetation model option (*ALL*), and the global temperature data (*DATA*). As can be seen by comparing *ALL:CONST* with *ALL*, when vegetation is held constant, this new

model responds to the specified climate forcings in a very similar fashion to the previous model version. When vegetation is allowed to change dynamically in response to climate changes however (*ALL:DYN*), there is a noticeable positive feedback to the climate system that results in an amplification of twentieth century climate warming by about a tenth of a degree.

This same vegetation-climate feedback can be seen in the land cover change only transient runs shown in Fig. 10. Including vegetation dynamics (*LCC:DYN*) increases the cooling signal from -0.14 °C (as in the case of the constant vegetation run: *LCC:CONST*) to -0.19 °C. The mechanism for this amplification can be seen in Fig. 11, which shows the difference in simulated Northern Hemisphere surface albedo between the

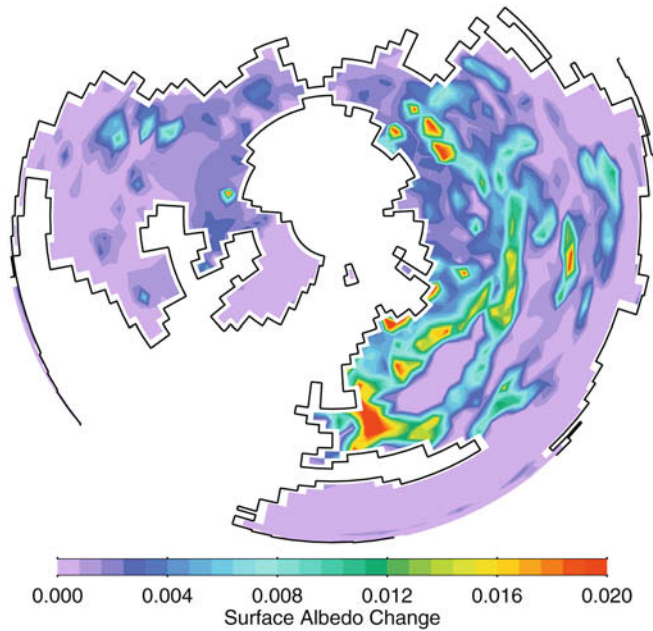


Fig. 11 Northern Hemisphere surface albedo change between *LU:DYN* and *LU:CONST* at present day. Increases in surface albedo reflect changes in high-latitude vegetation cover from forest vegetation types to grasses and shrubs in response to climate cooling

LCC:DYN and LCC:CONST transient runs at the year 2000. Higher surface albedo values are seen in LCC:DYN throughout Northern Asia, and to a lesser extent in North America. This increase follows directly from changes in high-latitude vegetation cover from forest vegetation types to grasses and shrubs in response to climate cooling. The globally averaged surface albedo increase is +0.0007, which is sufficient to account for the amplification of cooling between the two runs (see Table 3 for comparison). As in the case of the all-forcings model runs, vegetation dynamics act here as a positive feedback to the climate system, amplifying the effect of the specified forcing.

As stated in Sect. 4, in the case of prescribed vegetation, equilibrium and transient simulations of land cover change result in very similar global temperature

changes, a sign that the oceanic cooling commitment associated with land cover change is negligible. This is not the case however when vegetation is allowed to respond dynamically to changes in climate. Vegetation dynamics operate on decadal to centennial time scales, and as such introduce a new lag effect into the climate system that is not present when vegetation is prescribed or held constant.

Figure 12 shows the temperature difference over 1000 years of model integration between two equilibrium simulations of land cover change including dynamic vegetation. The temperature difference between present day and year 1700 simulations is seen to decrease rapidly, reaching $-0.19\text{ }^{\circ}\text{C}$ (the cooling reported for this model’s transient simulation of land cover change) at around 150 years of model integration. This cooling continues however, as vegetation distributions adjust to the new climate regime, approaching the equilibrium difference of $-0.32\text{ }^{\circ}\text{C}$ only after several hundred years. From this comparison, it is clear that the positive feedback to climate from dynamic vegetation in this model is a slow process that requires at least 400 or 500 years to achieve its full effect.

6 The net effect of land cover change

In all cases presented thus far, the UVic ESCM has demonstrated a radiative cooling as a result of surface albedo changes associated with historical land cover change. In this section we address the role that land cover changes have played in the global carbon cycle. Carbon emissions resulting from historical land cover change are well documented and are estimated to represent on the order of a quarter of all anthropogenic carbon emissions for recent decades (Bolin et al. 2000; Houghton 2003). This contribution to greenhouse gas forcing indicates that a significant portion of recent climate warming could be attributed to historical land cover change.

There have been some recent attempts to quantify the relative contribution of the biogeophysical effects (those associated with physical changes to the land surface) and

Fig. 12 Temperature difference between equilibrium simulations with present day and year 1700 land cover over 1000 years of model integration

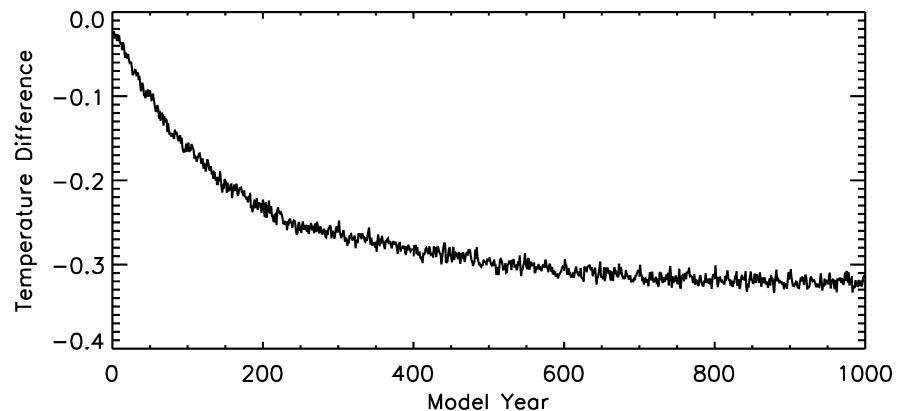
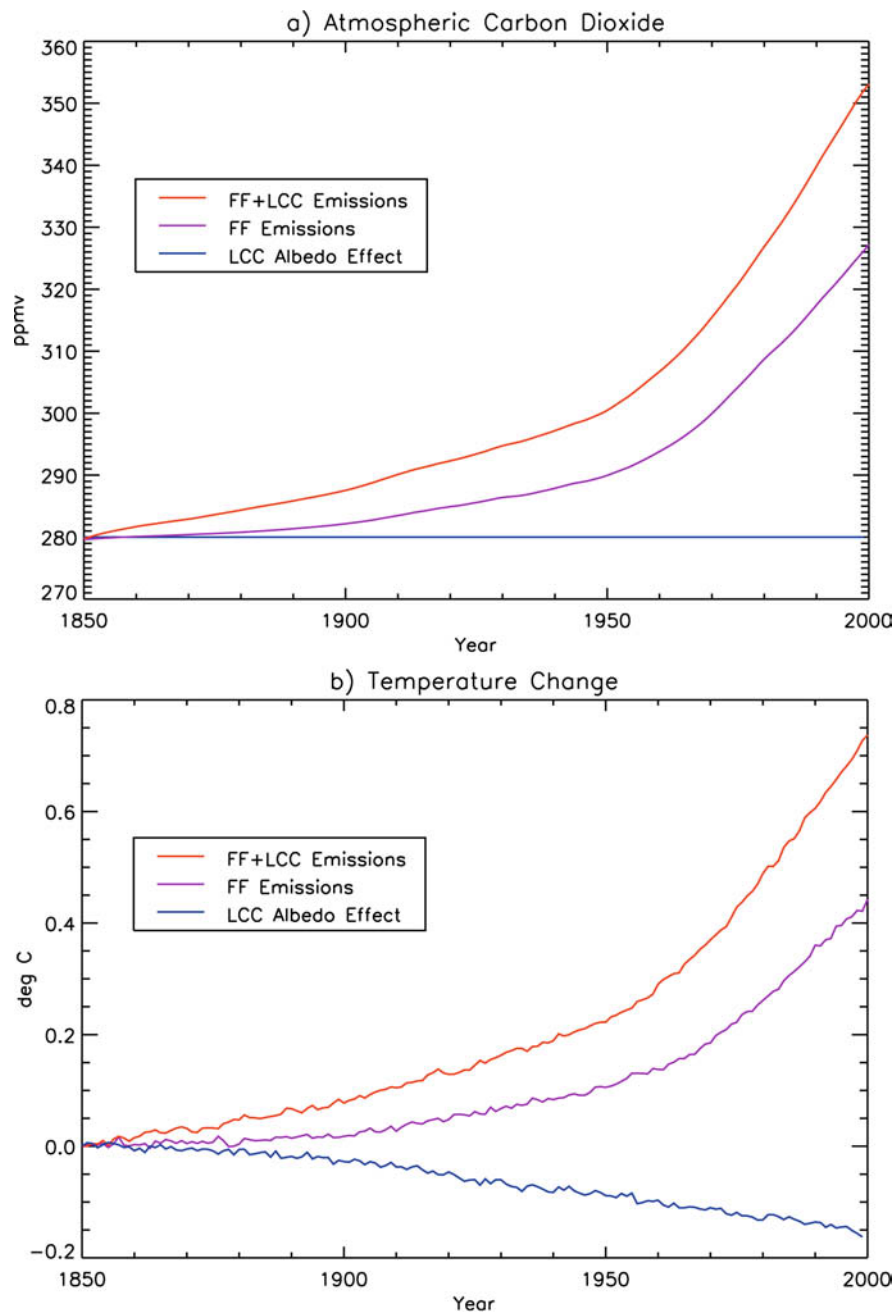


Fig. 13 Atmospheric carbon dioxide **a** and temperature change **b** from 1850 to 2000 resulting from transient runs forced by: fossil fuel emissions only (*purple line*) fossil fuel and land cover change emissions (*red line*) and land cover biogeophysical changes only (*blue line*)



biogeochemical effects (those resulting from emissions of greenhouse gases) of land cover change on global climate (Betts 2000; Claussen et al. 2001). These studies have used hypothetical scenarios of reforestation (Betts 2000) or of deforestation and afforestation (Claussen et al. 2001), and have found substantial regional variation in the magnitude and sign of the effect land cover change on climate when both biogeophysical and biogeochemical processes are considered.

In this section, we assess the net effect of historical land cover change on global and regional climate by comparing the magnitude of the albedo-induced cooling reported in previous sections, with the contribution of land cover change emissions of carbon dioxide to

twentieth century climate warming. The model experiments presented here use the UVic ESCM global carbon cycle model described in Sect. 2.5, allowing atmospheric carbon dioxide to be computed prognostically as a function of anthropogenic emissions, as well as terrestrial and oceanic carbon fluxes and sinks.

Results from two transient runs using this new carbon cycle model are shown in Fig. 13, along with output from the LCC:DYN transient run reported in Sect. 5. The first of these transient runs (FF Emissions) begins from a control integration with atmospheric carbon dioxide held fixed at 280 ppm and vegetation allowed to equilibrate in the absence of land cover change. Fossil fuel emissions from Marland et al. (2002) are then

specified from 1850 to present, and atmospheric CO₂ is allowed to respond freely to this forcing. The second transient run (FF+LCC Emissions) begins from a control integration where atmospheric carbon dioxide is held fixed at 280 ppm and vegetation is allowed to equilibrate under the constraint of imposed present day cropland distributions. Emissions from both fossil fuels and land cover change (Houghton 2003) are then specified from 1850 to present.

As can be seen in Fig. 13a, specifying only fossil fuel emissions results in a substantial underestimation of present day atmospheric carbon dioxide (327 ppm). Including land cover change emissions increases present day atmospheric carbon dioxide to 353 ppm, a value that is much closer to (but still somewhat less than) the observed CO₂ concentration of 365 ppm. Historical land cover change emissions from 1850 to 2000 total 156 GtC, compared to 275 GtC from fossil fuels. When land cover change emissions are included, 155 GtC is taken up by the terrestrial biosphere and 123 GtC is taken up by the ocean. This leaves an accumulation of 153 GtC in the atmosphere, slightly less than the Houghton et al. (2001) estimate of 176 ± 10 GtC. This discrepancy may in part result from an overestimation of pre-industrial terrestrial vegetation carbon (Meissner et al. 2003) or the exclusion of a dynamic nitrogen cycle (Cox 2001), both of which may account for an overestimation of terrestrial carbon uptake (historical and future terrestrial carbon dynamics are discussed more extensively in Matthews et al. submitted 2003). It is nevertheless clear that land cover change emissions are necessary to model accurately historical atmospheric carbon dioxide concentrations.

What is also apparent from Fig. 13b is that when land cover change emissions are included, the climate warming between 1850 and 2000 is increased by 0.3 °C compared to the case where only fossil fuel emissions are included. This global temperature change of 0.3 °C can be interpreted as the biogeochemical effect of historical land cover change, resulting from increased emissions of carbon dioxide. This can be compared to the biogeophysical effect of historical land cover change, reported to range from -0.06 °C to -0.22 °C from the year 1700 to 2000 in Sect. 3, and shown in Fig. 13b from 1850 to 2000 for the LCC:DYN run (-0.16 °C cooling). Considering the entire range of values found for the biogeophysical cooling, it can be concluded that the biogeochemical warming effect of historical land cover change emissions on globally averaged surface air temperature has exceeded the cooling effect of biogeophysical processes.

The climate response to these two competing effects of historical land cover change is also notable on a regional scale. In the carbon cycle model, carbon dioxide emissions are assumed to be instantaneously well mixed in the atmosphere, and as such, local warming does not represent local sources of carbon dioxide emissions. Nevertheless, there is a distinct regional pattern to both the warming associated with greenhouse gas emissions

(Fig. 14a) and the cooling generated by surface albedo changes (Fig. 14b). The regional patterns of warming/cooling shown here can be attributed largely to amplification by local feedbacks, such as sea-ice dynamics in the North Atlantic and Southern ocean, though in the case of Fig. 14b, the cooling pattern does also reflect the spatial distribution of land cover changes.

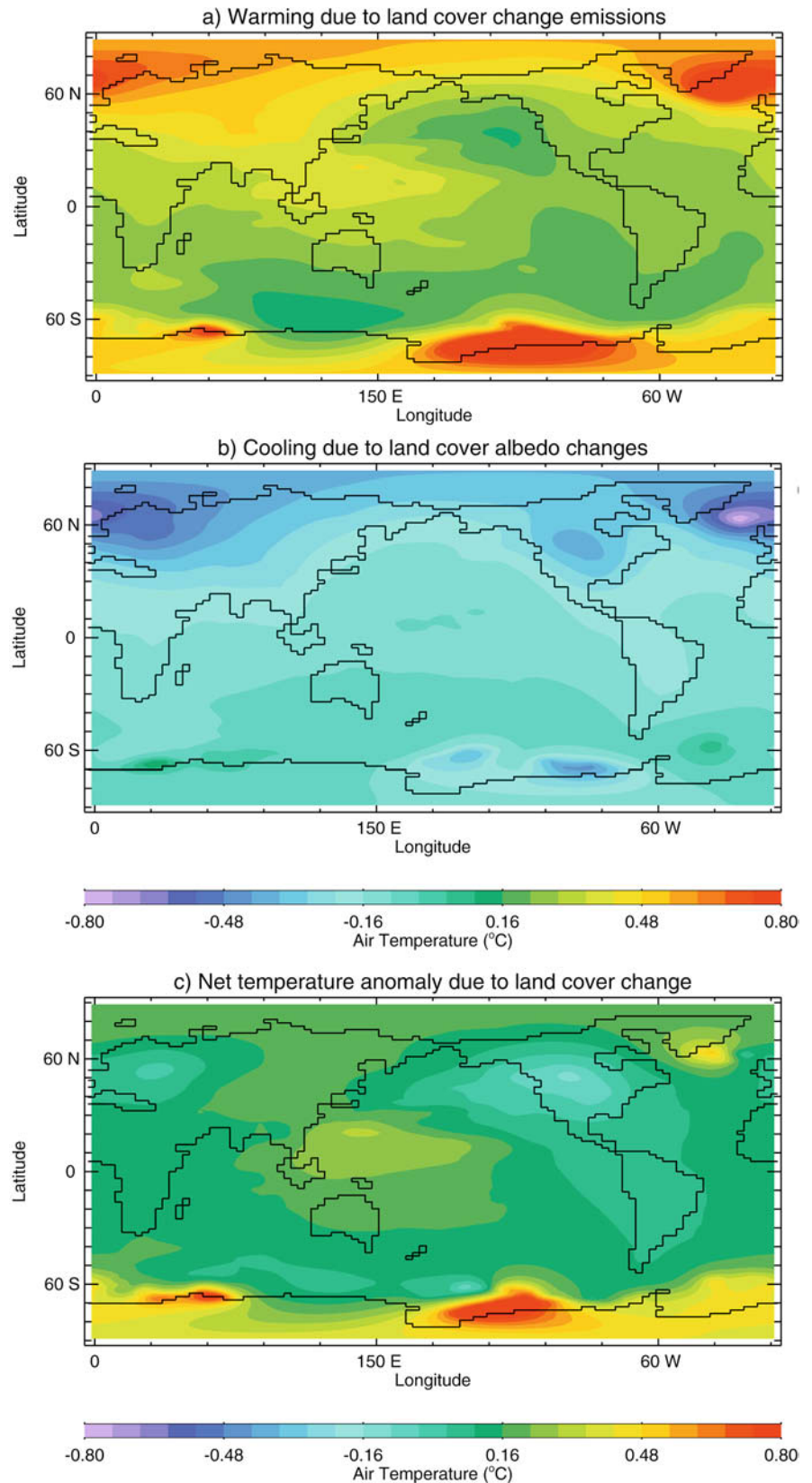
Assuming a linear additivity of climate responses, as was demonstrated in Sect. 4.1, we can combine Fig. 14a and b to determine the net effect of historical land cover change. Figure 14c thus represents the regional distribution of the net warming or cooling that results from both the biogeophysical and biogeochemical effects of historical land cover change. The net effect of land cover change reveals a distinct cooling over North America and very close to zero net change over Western Eurasia, with a warming most notable over the Pacific Ocean, at high northern latitudes and in the Southern Hemisphere. The globally averaged net effect of land cover change under this comparison results in a warming of 0.15 °C.

7 Conclusions

In this study we have focused on the role of historical land cover change in forcing the climate of the last 300 years. In a detailed sensitivity analysis using different datasets of land cover change and varying model configurations and parameters, we have found that the primary biogeophysical effect of historical land cover change has been to increase local surface albedos. This has resulted in a global cooling in the range of -0.06 °C to -0.22 °C for the range of equilibrium comparisons performed. We find in particular that the cooling that results from land cover change is highly sensitive in our model (and we would expect this to hold for other models as well) to the specified surface albedo for croplands, or other human-modified land cover types. The entire range of results reported in this section can in fact be reproduced simply by varying the specified cropland albedo value, with other model parameters proving to be of secondary importance.

In Sect. 4 we present results from transient climate simulations of the last 300 years. For the effect of land cover change, we have chosen an intermediate albedo value for croplands, resulting in a cooling of -0.13 °C from 1700 to present day. When compared to other anthropogenic (greenhouse gases and sulfate aerosols) and natural (volcanic aerosols, solar insolation and orbital changes) climate influences, we find that the biogeophysical effect of land cover change is of secondary importance to other anthropogenic forcings, though it is of comparable magnitude to smaller forcings such as solar variability. On short time scales, volcanic forcing far exceeds that of land cover change, but both account for a similar amount of cooling over decadal to centennial time scales. By comparing the effects of natural and anthropogenic climate influences, we find that

Fig. 14 Regional temperature anomalies due to: **a** land cover change emissions (biogeochemical effect), **b** land cover changes to surface albedo (biogeophysical effect) and **c** the net result of both the biogeochemical and biogeophysical effects of land cover change



the warming trend of the late twentieth century is well simulated by the combined effects of anthropogenic activities, whereas warming and cooling trends in the

earlier portion of the temperature record are likely attributable to a combination of natural and anthropogenic climate change.

In Sect. 4.2, we find that the effect of land cover change is too small to be detectable in either twentieth century temperature data or hemispherically averaged proxy data. This result suggests that while it is important to include land cover change in simulations of recent climate change, the effect of this forcing is small compared to natural climate variability and other anthropogenic climate changes. The issue of detection is complicated by the uncertainties associated with estimates of land cover change as well as its coupled biogeophysical and biogeochemical effects on climate. It is perhaps not surprising that the albedo-induced cooling effect alone is not readily detectable in twentieth century observations.

When vegetation dynamics are included, as in Sect. 5, we see that the results presented in previous sections are amplified by a positive feedback between vegetation dynamics and the climate system. In the case of land cover change, vegetation dynamics increase the cooling signal from -0.14 °C to -0.19 °C between 1700 and present day. We conclude from these transient runs that twentieth century climate change has been forced primarily by changes in greenhouse gases, but that other forcings and internal model feedbacks contribute to a very realistic simulation of climate change over the past 300 years. We also find that the positive vegetation feedback introduces a significant lag effect into the climate model, resulting in a much larger equilibrium temperature difference (-0.32 °C) associated with land cover change than that found in the transient simulations (-0.19 °C).

In the final part of this study (Sect. 6), we address the question of the net effect of historical land cover change, including both biogeochemical and biogeophysical processes. We find that including land cover change emissions in a transient climate simulation of the past 150 years amplifies greenhouse warming by 0.3 °C on the global average. This increase exceeds the biogeophysical cooling found over the same period (-0.16 °C). We therefore conclude that the net effect of land cover change has been to increase global temperatures over the last 150 years by an amount of the order 0.15 °C. We further note that in some geographical regions, particularly over Northern Hemisphere continents, the cooling influence of land cover change has dominated, while over most of the rest of the globe, the net effect has been warming.

These conclusions point to the important role that human land cover changes have played in observed climate change. It is clear that historical land cover change has had regionally varied and significant implications for global temperatures, and that when included in transient simulations of recent climate change, land cover changes help to improve model simulations of the historical temperature record. Including the effect of land cover change emissions is of particular importance, as their contribution to recent climate warming has been notable. In future work, when considering the implications of carbon cycle feedbacks to climate, it will be critical to

include the combined effects of land cover change on surface parameters, global carbon sinks and carbon dioxide emissions.

Acknowledgements The authors wish to thank E. Wiebe, T. Ewen and S. Turner for assistance, advice, and editorial comments as well as M. Claussen and B. Govindasamy for their thoughtful and useful suggestions. Funding support from the Climate Variability and Predictability Research Program (CLIVAR), the Canadian Foundation for Climate and Atmospheric Studies (CFCAS) and the National Science and Engineering Research Council (NSERC) is gratefully acknowledged.

8 Appendix 1

8.1 Modified bucket model description

In the standard bucket model, soil moisture (W) is calculated using a budget approach:

$$\frac{\delta W}{\delta t} = P_R + S_M - E - R \quad (8)$$

Inputs to the soil moisture bucket come in the form of precipitation (P_R) and snowmelt (S_M); outputs take the form of evapotranspiration (E) and runoff (R).

The simplest parametrisation of evaporation is that used in the original version of the bucket model, and is based on a bulk formulation of potential evaporation and the specification of a surface resistance that reduces evaporation from its potential rate in cases where soil moisture is limiting. Following the methodology of a number of other land-surface models (see e.g. Dickinson 2001; Zeng et al. 2000; Cox et al. 1999), we improve on the original bulk formulation of evaporation by parametrizing evapotranspiration as:

$$E_r = \rho_a \frac{\beta}{r_a + r_s} [q_{sat}(T_s) - q_a] \quad (9)$$

where ρ_a is the density of air, $q_{sat}(T_s)$ is the saturation specific humidity of air at the surface temperature and q_a is the atmospheric specific humidity. The term β imposes a damp on evaporation as water availability decreases, and is calculated as $\beta = (W/W_0)^{1/4}$ where W is the soil moisture content and W_0 is the soil water holding capacity or bucket depth (15 cm).

The resistance terms r_a and r_s are the aerodynamic and surface resistances, which impose physical and physiological constraints on evapotranspiration. The first of these (r_a) is simply a function of the Dalton number for evaporation and the surface wind speed: $r_a = (C_D U)^{-1}$. The Dalton number is calculated from a specified surface roughness length (z_0) according to the methodology of Brutsaert (1982):

$$C_D = k^2 \left(\ln \frac{z}{z_0} \right)^{-1} \left(\ln \frac{z}{z_{0q}} \right)^{-1} \quad (10)$$

where z is a reference height ($z = 10$ m) and k is the von Karman constant ($k = 0.4$). The roughness length for moisture (z_{0q}) is calculated as $z_{0q} = e^{-2} z_0$.

When snow is present in a grid cell, the surface albedo is determined on the basis of the underlying vegetation albedo and a fractional snow cover. Using the vegetation snow-masking depths, the fractional area of snow in a grid cell (A_{snow} , constrained between 0.0 and 1.0) is calculated as:

$$A_{snow} = \max \left[H_{snow}, \frac{T_{air} - T_{start}}{T_{end} - T_{start}} \right] \cdot \frac{1}{SMD} \quad (11)$$

where T_{start} and T_{end} are set to -5 °C and -10 °C respectively, T_{air} is the atmospheric temperature, H_{snow} is the snow height in metres

(Weaver et al. 2001) and *SMD* is a vegetation-type dependant snow-masking depth. The albedo for snow is then applied to this fractional area, with the underlying snow-free albedo given to the remaining portion of the grid cell.

Surface temperature is calculated from the energy balance equation:

$$R_{NET} = LE + SH \quad (12)$$

R_{NET} is the net radiation at the surface (comprising downward shortwave and upward longwave), LE is the latent heat from evaporation and SH is the sensible heat exchange. There is no heat storage in the land surface.

References

- Bauer E, Claussen M, Brovkin V (2003) Assessing climate forcings of the Earth system for the past millenium. *Geophys Res Lett* 30: 9-1-9-4
- Berger AL (1978) Long-term variations of daily insolation and quaternary climate change. *J Atmos Sci* 35: 2362–2367
- Bertrand C, France Loutre M, Crucifix M, Berger A (2002) Climate of the last millennium: a sensitivity study. *Tellus* 54A: 221–244
- Betts RA (2000) Offset of the potential carbon sink from boreal forestation by decreases in surface albedo. *Nature* 408: 187–190
- Betts RA (2001) Biogeophysical impacts of land use on present-day climate: near surface temperature and radiative forcing. *Atmos Sci Lett* 1: doi:10.1006/asle.2001.0023
- Bitz CM, Holland MM, Weaver AJ, Eby M (2001) Simulating the ice-thickness distribution in a coupled climate model. *J Geophys Res* 106: 2441–2464
- Bolin B, Sukumar R, Ciais P, Cramer W, Jarvis P, Kheshgi H, Nobre C, Semenov S, Steffen W (2000) Global perspective. In: Watson RT, et al. (eds) Land use, land-use change, and forestry: a special report of the Intergovernmental Panel on Climate Change, Cambridge University Press, Cambridge, UK, pp 23–51
- Bounoua L, De Fries R, Collatz G, Sellers P, Khan H (2002) Effects of land cover conversion on surface climate. *Clim Change* 52: 29–64
- Brovkin V, Ganopolski A, Claussen M, Kubatzki C, Petoukhov V (1999) Modelling climate response to historical land cover change. *Global Ecol Biogeogr* 8: 509–517
- Brutsaert W (1982) Evaporation into the atmosphere. D. Reidel, Boston, USA
- Charlson R, Langner J, Rodhe H, Leovt C, Warren G (1991) Perturbation of the Northern Hemisphere radiative balance by backscattering from anthropogenic sulfate aerosols. *Tellus* 43AB: 152–163
- Chase T, Pielke R, Kittel T, Nemani R, Running S (2000) Simulated impacts of historical land cover changes on global climate in northern winter. *Clim Dyn* 16: 93–105
- Chase T, Pielke R, Kittel T, Zhao M, Pitman A, Running S, Nemani R (2001) Relative climatic effects of landcover change and elevated carbon dioxide combined with aerosols: a comparison of model results and observations. *J Geophys Res* 106: 31,685–31,691
- Clapp RB, Hornberger GM (1978) Empirical equations for some soil hydraulic properties. *Water Resources Res* 14(4): 601–604
- Claussen M, Brovkin V, Ganopolski A (2001) Biogeophysical versus biogeochemical feedbacks of large-scale land cover change. *Geophys Res Lett* 28: 1011–1014
- Cox PM (2001) Description of the “TRIFFID” dynamic global vegetation model. Technical Note 24, Hadley Center, Meteorological Office, UK
- Cox P, Betts R, Bunton C, Essery R, Rowntree P, Smith J (1999) The impact of new land surface physics on the GCM simulation of climate and climate sensitivity. *Clim Dyn* 15: 183–203
- Cramer W, Bondeau A, Woodward FI, Prentice IC, Betts RA, Brovkin V, Cox PM, Fisher V, Foley JA, Friend AD, Kucharik C, Lomas MR, Ramankutty N, Sitch S, Smith B, White A, Young-Molling C (2001) Global response of terrestrial ecosystem structure and function to CO₂ and climate change: results from six dynamic global vegetation models. *Glob Change Biol* 7: 357–373
- Crowley TJ (2000) Causes of climate change over the past 1000 years. *Science* 289: 270–277
- De Fries R, Townsend J (1994) NDVI -derived land cover classification at global scales. *Int J Rem Sen* 15: 3567–3586
- Dickinson RE (2001) Biosphere-Atmosphere Transfer Scheme (BATS) version 1e as coupled to the NCAR Community Climate Model. NCAR Technical Note NCAR TN 387 STR
- Flato GM, Boer GJ (2001) Warming asymmetry in climate change simulations. *Geophys Res Lett* 23: 195–198
- Folland C, Rayner N, Brown S, Smith SS, Parker D, Macadam I, Jones P, Jones R, Nicholls N, Sexton D (2001) Global temperature change and its uncertainties since 1861. *Geophys Res Lett* 28: 2621–2624
- Gill AE (1982) Atmosphere-ocean dynamics. Academic Press, New York, USA
- Govindasamy B, Duffy P, Caldeira K (2001) Land use change and Northern Hemisphere cooling. *Geophys Res Lett* 28: 291–294
- Graves CE, Ho Lee W, North GR (1993) New parametrizations and sensitivities for simple climate models. *J Geophys Res* 98: 5025–5036
- Haney RL (1971) Surface thermal boundary conditions for ocean circulation models. *J Phys Ocean* 1: 241–248
- Hansen JE, Sato M, Lacis A, Ruedy R, Tegen I, Matthews E (1998) Climate forcings in the industrial era. *Proc Natl Acad Sci USA* 95: 12,753–12,758
- Hegerl GC, Crowley TJ, Baum SK, Yul Kim K, Hyde WT (2003) Detection of volcanic, solar and greenhouse gas signals in paleo-reconstructions of Northern Hemispheric temperature. *Geophys Res Lett* 30:461–464
- Houghton J et al (eds) (2001) Climate change 2001: the scientific basis. Cambridge University Press, Cambridge, UK
- Houghton R (2003) Revised estimates of the annual net flux of carbon to the atmosphere from changes in land use and land management 1850–2000. *Tellus* 55B: 378–390
- Jones GS, Tett SF, Stott PA (2003) Causes of atmospheric temperature change 1960–2000: a combined attribution analysis. *Geophys Res Lett* 30: 32-1–32-4
- Jones P (1993) Hemispheric surface air temperature variations: a reanalysis and update to 1993. *J Clim* 7: 1794–1802
- Klein Goldewijk K (2001) Estimating global land use change over the past 300 years: the HYDE database. *Global Biogeochem Cyc* 15: 415–433
- Koch D (2001) Transport and direct radiative forcing of carbonaceous and sulfate aerosols in the GISS GCM. *J Geophys Res* 106: 20,311–20,332
- Lean J, Beer J, Bradley R (1995) Reconstruction of solar irradiance since 1610: implications for climate change. *Geophys Res Lett* 22: 3195–3198
- Manabe S (1969) Climate and the ocean circulation 1. The atmospheric circulation and the hydrology of the earth's surface. *Mon Weather Rev* 97(11): 739–774
- Mann M, Bradley R, Hughes M (1999) Northern Hemisphere temperature during the past millenium: inferences, uncertainties and limitations. *Geophys Res Lett* 26: 759–762
- Marland G, Boden T, Andres R (2002) Global, regional, and national annual CO₂ emissions from fossil-fuel burning, cement production, and gas flaring: 1751–1999. CDIAC NDP-030, Carbon Dioxide Information Analysis Center
- Matthews HD, Weaver AJ, Eby M, Meissner KJ (2003) Radiative forcing of climate by historical land cover change. *Geophys Res Lett* 30: 27-1–27-4
- Meissner KJ, Weaver AJ, Matthews HD, Cox PM (2003) The role of land-surface dynamics in glacial inception: a study with the UVic Earth System Climate Model. *Clim Dyn* 21:519–537

- Myhre G, Myhre A (2003) Uncertainties in radiative forcing due to surface albedo changes caused by land-use changes. *J Clim* 19: 1511–1524
- Pacanowski R (1995) MOM 2 documentation user's guide and reference manual, GFDL ocean group Technical Report. NOAA, GFDL, Princeton, USA
- Petit JR, Jouzel J, Raynaud D, Barnola J, Basile I, Bender M, Chappellaz J, Davis M, Delaygue G, Delmotte M, Kotlyakov V, Legrand M, Lipenkov V, Lorius C, Pépin L, Ritz C, Saltzman E, Stievenard M (1999) Climate and atmospheric history of the past 420,000 years from the Vostok ice core, Antarctica. *Nature* 399: 429–436
- Ramankutty N, Foley JA (1999) Estimating historical changes in land cover: croplands from 1700 to 1992. *Global Biogeochem Cyc* 13: 997–1027
- Ramaswamy V, Chen C (1997) Linear additivity of climate response for combined albedo and greenhouse perturbations. *Geophys Res Lett* 24: 567–570
- Ramaswamy V, Boucher O, Haigh J, Hauglustaine D, Harwood J, Myhre G, Nakajima T, Shi G, Solomon S (2001) Radiative forcing of climate change. In: Houghton J et al. (eds) *Climate change 2001: the scientific basis*. Cambridge University Press, Cambridge, UK, pp 349–416
- Robock A (1994) Review of year without a summer? world climate in 1816. *Clim Change* 26: 105–108
- Robock A (2000) Volcanic eruptions and climate. *Rev Geophys* 38: 191–219
- Robock A, Free M (1995) Ice cores as an index of global volcanism from 1850 to the present. *J Geophys Res* 100: 11,549–11,567
- Sato M, Hansen J, McCormick M, Pollack J (1993) Stratospheric aerosol optical depth, 1980–1990. *J Geophys Res* 98: 22,987–22,994
- Schlesinger ME, Malyshev S (2001) Changes in near-surface temperature and sea-level for the post-SRES CO₂-stabilization scenarios. *Integrated Assessment* 2: 95–199
- Sellers P, Meeson B, Closs J, Collatz J, Corprew F, Dazlich D, Hall F, Kerr Y, Koster R, Los S, Mitchell K, McManus J, Myers D, Sun KJ, Try P (1996) The ISLSCP initiative I global datasets: surface boundary conditions and atmospheric forcings for land-atmosphere studies. *B Am Meteorol Soc* 77(9): 1987–2005
- Stott P, Tett S, Jones G, Allen M, Ingram W, Mitchell J (2001) Attribution of twentieth century temperature change to natural and anthropogenic causes. *Clim Dyn* 17: 1–21
- Tegen I, Koch D, Lacis AA, Sato M (2000) Trends in tropospheric aerosol loads and corresponding impact on direct radiative forcing between 1950 and 1990: a model study. *J Geophys Res* 105: 26,971–26,989
- Tett SFB, Stott PA, Allen MR, Ingram WJ, Mitchell JFB (1999) Causes of twentieth century temperature change near the Earth's surface. *Nature* 399: 569–572
- Weaver AJ, Eby M, Wiebe EC, Bitz CM, Duffy PB, Ewen TL, Fanning AF, Holland MM, MacFadyen A, Matthews HD, Meissner KJ, Saenko O, Schmittner A, Wang H, Yoshimori M (2001) The UVic Earth System Climate Model: model description, climatology and applications to past, present and future climates. *Atmos Ocean* 39: 361–428
- Wilson M, Henderson-Sellers A (1985) A global archive of land cover and soils data for use in general circulation climate models. *J Climatol* 5: 119–143
- Zeng N, Neelin JD, Chou C, Wei-Bing Lin J, Su H (2000) Climate and variability in the first quasi-equilibrium tropical circulation model. In: Randall DA (ed) *General circulation model development*, Academic Press, New York, USA, pp 457–488
- Zhao M, Pitman A, Chase T (2001) The impact of land cover change on the atmospheric circulation. *Clim Dyn* 17: 467–477